Human Factor VIIa and Its Complex with Soluble Tissue Factor: Evaluation of Asymmetry and Conformational Dynamics by Ultracentrifugation and Fluorescence Anisotropy Decay Methods†

Evan Waxman,‡ William R. Laws,‡ Thomas M. Laue,§ Yale Nemerson,*,‡,∥ and J. B. Alexander Ross*,‡

Departments of Biochemistry and Medicine, Mount Sinai School of Medicine of the City University of New York, New York, New York 10029, and Department of Biochemistry, University of New Hampshire, Durham, New Hampshire 03824

Received September 10, 1992; Revised Manuscript Received January 6, 1993

ABSTRACT: Ultracentrifugation and fluorescence anisotropy decay measurements were used to evaluate the asymmetry and conformational dynamics of human blood clotting enzyme VIIa (VIIa) and the complex it forms with a soluble truncation mutant of human tissue factor (sTF) which acts as an essential cofactor for VIIa. Sedimentation velocity experiments showed that both VIIa and the sTF·VIIa complex are highly asymmetric. In each case, the friction ratio, f/f_{sphere}, is consistent with a family of general ellipsoids ranging from prolate to oblate. Fluorescence anisotropy decay experiments were used to limit the family of ellipsoids which can describe the hydrodynamic behavior of VIIa and sTF·VIIa. For both VIIa and the sTF·VIIa complex, the oblate ellipsoid of revolution was eliminated. In addition, the fluorescence anisotropy decay data clearly show that upon binding sTF·VIIa loses a segmental motion involving a domain containing the active site of the enzyme. This suggests that sTF causes a stabilization of a limited range of VIIa conformations. This stabilization may be important for proper recognition of the TF·VIIa substrate, factor X.

The complexation of factor VIIa (VIIa)[1] with membrane-bound tissue factor (TF) is a critical step in the initiation of blood coagulation. TF is a transmembrane glycoprotein consisting of an extracellular domain (residues 1–219), a single transmembrane domain (residues 220–242), and a cytoplasmic domain (residues 243–263) which contains a half-cysteine residue thioesterified to palmitate or stearate [for review, see Bach (1988)]. When complexed with TF, the serine protease activity of VIIa toward its natural substrate, factor X (X), is increased by many orders of magnitude (Silverberg et al., 1977).

In vivo, complexation of TF and VIIa takes place at the vascular wall [for review, see Nemerson and Turitto (1991)]. Near the wall, viscous drag is exerted by the stationary vascular surface radially and by the bulk of the flowing blood medially. In this way, high shear forces are generated. An asymmetric molecule *in solution near the wall* should thus tend to align parallel to the direction of flow. If the molecule is *anchored at the vascular wall*, it should experience forces that may be important for determining conformation. This suggests two mechanisms by which a flowing environment could affect the kinetics of blood coagulation and other reactions that take place at the vascular surface.

In this paper, we present results from sedimentation and fluorescence anisotropy measurements that clearly demonstrate that VIIa and the complex it forms with sTF, a soluble truncation mutant of TF, are both highly asymmetric. In addition, we have established that the binding of sTF to VIIa induces a conformational change in VIIa that leads to a loss in the segmental flexibility of VIIa in the domain containing the active site. In doing so, we have combined measurement of translational and rotational hydrodynamic properties in a useful way that may serve as a template for studies of other protein systems where asymmetry and flexibility would be of interest.

EXPERIMENTAL PROCEDURES

Experimental Approach. In the absence of X-ray crystal structure models for TF, VIIa, or the complex they form (TF·VIIa), there is a need to use other physical methods to assess their three-dimensional structures. The classical method for examining the global structure of a protein in solution is by assessment of its hydrodynamic properties using ultracentrifugation. Sedimentation equilibrium and sedimentation velocity experiments provide the molecular weight and the translational frictional coefficient of the macromolecule. The translational frictional coefficient, however, is a single parameter which depends on the size, shape, and flexibility of the molecule. Thus, it is impossible to distinguish between oblate (discus shaped) and prolate (cigar shaped) models using sedimentation velocity alone. Likewise, it is impossible to distinguish a flexible asymmetric molecule from a rigid molecule of lower asymmetry.

In this paper, we demonstrate that time-resolved fluorescence anisotropy decay measurements provide additional information that can reduce the centrifuge determined range of possible shapes that are consistent with the hydrodynamic behavior of VIIa and the sTF·VIIa complex.

Figure 1 outlines the flow of information—data, calculations, and assumptions—that we used to place limits on the semiaxes of the general ellipsoid (Figure 2) that best represents the hydrodynamic behavior of VIIa and sTF·VIIa. Our initial observation is that the steady-state anisotropy of an active-site, dansyl-labeled VIIa prepared for thermodynamic studies (Waxman et al., 1992) indicates that neither VIIa nor sTF·VIIa is well represented by a monomeric sphere. To address whether the steady-state anisotropy reflects higher

† Supported in parts by Grants HL-29019 and GM-39750 from the National Institutes of Health and by Grant DIR-9002027 from the National Science Foundation.

* Authors to whom correspondence should be addressed.

‡ Department of Biochemistry, Mount Sinai School of Medicine, New York, NY 10029.

§ Department of Biochemistry, University of New Hampshire, Durham, NH 03824.

∥ Department of Medicine, Mount Sinai School of Medicine, New York, NY 10029.

[1] Abbreviations: VIIa, factor VIIa; X, factor X; sTF, soluble tissue factor; FFRCk, D-Phe-L-Phe-Arg chloromethyl ketone; DF-VIIa, dansyl-D-Phe-L-Phe-Arg-labeled VIIa; SDS–PAGE, sodium dodecyl sulfate–polyacrylamide gel electrophoresis.

0006-2960/93/0432-3005$04.00/0

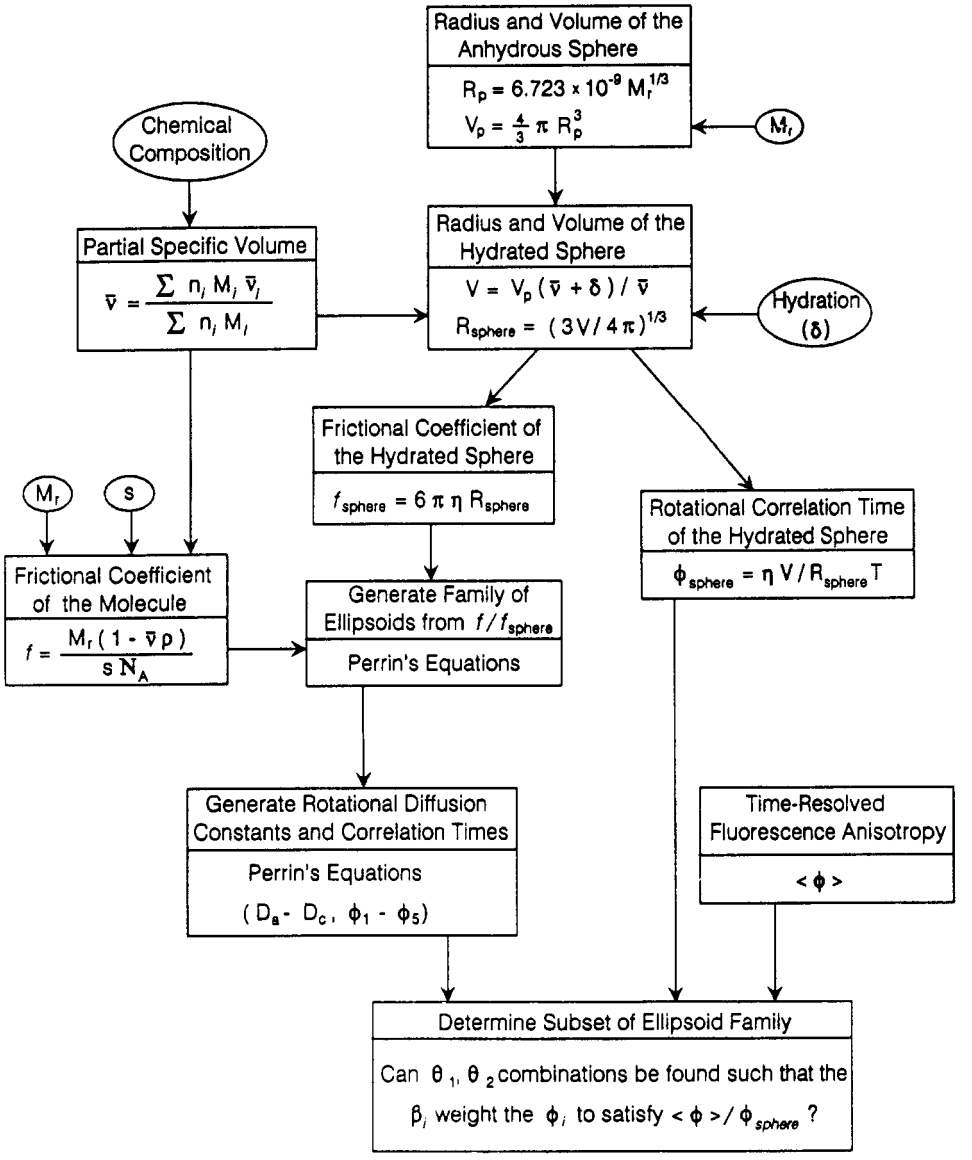

FIGURE 1: Flow diagram for evaluation of hydrodynamic parameters showing inputs, assumptions, procedures, and equations where appropriate. Steps are explained fully in Experimental Procedures.

order associations of these molecules, we performed equilibrium ultracentrifugation experiments. Sedimentation velocity experiments were then performed to evaluate the deviation of the molecules from rigid spheres. Using equations derived by Perrin (1934), we generated a family of ellipsoids that are consistent with the centrifuge data for VIIa and sTF·VIIa. As discussed below, time-resolved fluorescence anisotropy experiments were then used to place additional limits on the family of ellipsoids and to distinguish between changes in the translational frictional coefficient due to asymmetry or those due to increased rigidity. This approach has been previously suggested by Small and Isenberg (1977) and Stafford and Szent-Györgyi (1978).

Calculation of R_{sphere}, the Radius of the Hydrated Stokes' Sphere. A useful and commonly applied first step in the evaluation of hydrodynamic observables is the calculation of values expected if the molecule were a rigid sphere. In this way, considerations of molecular size are factored out and only shape parameters—asymmetry and flexibility—need be considered. The first step shown in Figure 1 is the calculation of R_p, the radius of an anhydrous sphere with a molecular weight equal to that of the molecule of interest. For this we used the empirical equation

$$R_p = (6.723 \times 10^{-9}) M_r^{1/3} \quad (1)$$

where M_r is the molecular weight obtained from equilibrium centrifugation (Teller, 1976). This relationship is based on packing volumes observed in X-ray crystallographic structures of protein–protein complexes. The anhydrous molecular volume, V_p, can be calculated from R_p. It has been shown that the classical textbook formation,

$$R_0 = \sqrt[3]{\frac{3 M_r \bar{v}}{4 \pi N_A}} \quad (2)$$

where N_A is Avogadro's number and $\bar{v}$ is the partial specific volume of the protein, underestimates the radii and leads to overestimates of the axial ratios in subsequent calculations (Laue et al., 1992).

The hydration, δ, is used in the next step to generate V, the volume of the *hydrated* sphere.

$$V = V_p \left(\frac{\bar{v} + \delta}{\bar{v}} \right) \quad (3)$$

$\bar{v}$ is estimated using the method of Cohn and Edsall (1943;

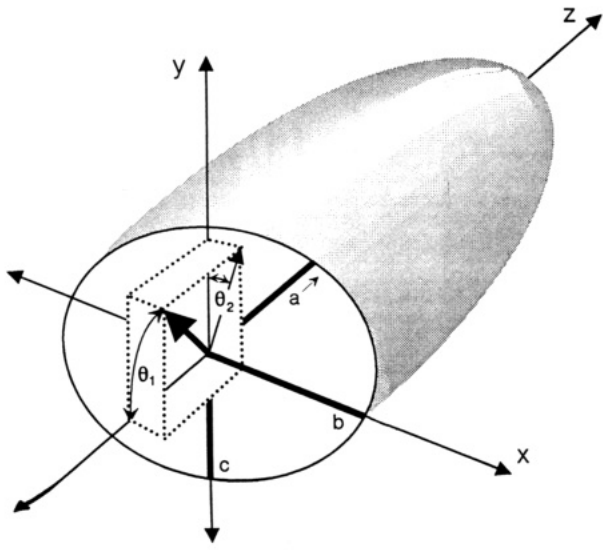

FIGURE 2: Representation of a general ellipsoid. The semiaxes of the ellipsoid are a, b, and c with $a \geq b \geq c$. We assume that the absorbance and emission transition dipole moments of the fluorophore, represented by the bold arrow, are coincident. θ_1 and θ_2 are the angles defining the orientation of the dipole moments with respect to the molecular axes. θ_1 is the angle to the major semiaxis a, and θ_2 is defined by the projection onto the plane of the b and c semiaxes.

Laue et al., 1992)

$$\bar{v} = \frac{\Sigma n_i M_i \bar{v}_i}{\Sigma n_i M_i} \tag{4}$$

where n_i, M_i, and $\bar{v}_i$ are the number of moles, molecular weight, and partial specific volumes, respectively, for the components—amino acids and carbohydrates—which make up the protein. For the purposes of this development, δ was estimated at 0.280 g of H_2O/g of protein. This value is an average of data from sedimentation velocity and small-angle X-ray scattering experiments for a group of proteins with molecular weights less than 100 000 (Pessen & Kumosinski, 1985). R_{sphere}, the radius of the *hydrated* Stokes' sphere, is easily calculated from V.

Sedimentation Velocity: Calculation of f_{sphere}. For a rigid, spherical particle, Stokes' law predicts that the translational frictional coefficient is given by

$$f_{sphere} = 6\pi\eta R_{sphere} \tag{5}$$

where η is the solvent viscosity.

Evaluation of f and Calculation of the Friction Ratio. The rate, v, at which a molecule sediments in a centrifugal field $\omega^2 r$ is given by the Svedberg equation

$$s = \frac{v}{\omega^2 r} = \frac{M_r(1 - \bar{v}\rho)}{N_A f} \tag{6}$$

where s is the sedimentation coefficient for the molecule, f is the frictional coefficient, ρ is the solvent density, ω is the angular velocity, and r is the distance of the molecule from the center of the field.

An asymmetric particle will have a frictional coefficient greater than that of a spherical particle of the same volume. Thus, the friction ratio, f/f_{sphere}, is often used to calculate the axial ratios for prolate and oblate ellipsoids which are consistent with the behavior of the molecule in the centrifuge. There is no reason, however, to believe that a protein is well represented by either an oblate or a prolate ellipsoid, and, in fact, for a given friction ratio the oblate and prolate models provide the most extreme cases of deviation from a sphere. If we take the semiaxes of an ellipsoidal structure to be a, b, and c with $a > b > c$ (Figure 2), then for a rigid particle the friction ratio defines a family of rigid ellipsoids ranging in flatness (b/c) and elongation (a/b) from the oblate case to the prolate. The family of ellipsoids consistent with a given friction ratio can be generated by numerical evaluation of Perrin's equation (Perrin, 1934) as outlined by Small and Isenberg (1977). Initially, semiaxis a is set equal to semiaxis b. Semiaxis c is numerically evaluated to obtain the initial ratio for the oblate case. Semiaxis c is then numerically evaluated for increasing values of a/b until the prolate case, $b = c$, is reached. The result of this procedure is a table of b/c versus a/b for ellipsoids with the experimentally-determined friction ratio.

If an asymmetric molecule is not rigid, any segmental flexibility will lower the friction ratio compared to that of the fully extended molecule. Sedimentation velocity experiments measure the time-averaged shape of the molecule. Thus, the friction ratio defines a family of ellipsoids that represent the time-averaged shape of the molecule and it is impossible, using sedimentation methods alone, to distinguish between a highly asymmetric flexible molecule and a rigid molecule of lower asymmetry.

Fluorescence Anisotropy: Calculation of ϕ_{sphere}. For fluorophores bound to a macromolecule, the rate at which the chromophore rotates, and therefore the polarization of its emitted light, will be affected by the size, shape, and flexibility of the macromolecule as well as by the orientation of the fluorophore to the macromolecular axes. For a fluorophore rigidly attached to a rigid spherical molecule, the rotational correlation time, ϕ_{sphere}, may be calculated from the Stokes–Einstein equation

$$\phi_{sphere} = \frac{\eta V}{RT} \tag{7}$$

In this equation, R is the gas constant, η is the solution viscosity, and T is the temperature.

Evaluation of $\langle\phi\rangle$ and the Rotational Ratio. Two types of experiments are typically performed to assess the rotational correlation time, ϕ, of a fluorophore. In a steady-state fluorescence anisotropy experiment, the solution is excited continuously and fluorescence is detected through vertically and horizontally oriented polarizers. The amount of depolarization is expressed as the steady-state anisotropy, $\langle r\rangle$, given by

$$\langle r\rangle = \frac{I_v - I_h}{I_v + 2I_h} \tag{8}$$

where I_v and I_h are the intensities detected through vertical and horizontal polarizers when vertical light is used to excite the sample. The measured steady-state anisotropy will be

$$\langle r\rangle_{sphere} = \frac{\langle r\rangle_0}{1 + \tau/\phi_{sphere}} \tag{9}$$

where $\langle r\rangle_0$ is the zero-point or "frozen" anisotropy extrapolated back to infinite solvent viscosity and τ is the intensity lifetime of the fluorophore. The degree to which a macromolecule deviates from a rigid sphere may be assessed by comparing the measured $\langle r\rangle$ to $\langle r\rangle_{sphere}$. Asymmetry will cause the measured $\langle r\rangle$ to shift toward $\langle r\rangle_0$ and to exceed $\langle r\rangle_{sphere}$. If the macromolecule is not rigid or the fluorophore has depolarizing motions independent of the macromolecule, these segmental motions will cause the measured $\langle r\rangle$ to shift toward 0 and to be less than $\langle r\rangle_{sphere}$. In addition, the orientation of the probe with respect to the macromolecular axes is important in determining the degree to which asymmetry and flexibility cause deviation from $\langle r\rangle_{sphere}$ (see below).

In a time-resolved fluorescence anisotropy experiment, the sample is repetitively pulsed with polarized light. By analogy with eq 8, the time dependence of the depolarization due to rotation is measured as

$$r(t) = \frac{I_v(t) - I_h(t)}{I_v(t) + 2I_h(t)} \tag{10}$$

For a fluorophore rigidly attached to a rigid spherical molecule, the anisotropy decay law is given by

$$r(t) = r_0 e^{-t/\phi_{sphere}} \tag{11}$$

where r_0 is the anisotropy extrapolated back to time zero. For a fluorophore rigidly attached to a nonspherical molecule, the anisotropy decay is considerably more complicated. It has been shown that the anisotropy decay law for an ellipsoidal molecule is a sum of five exponentials (Tao, 1969; Belford et al., 1972) given by

$$r(t) = \sum_{i=1}^{5} \beta_i e^{-t/\phi_i} \tag{12}$$

Calculations of the relative values of the correlation times of these exponentials for ellipsoids of varying axial ratios show that only three values of ϕ_i are sufficiently distinct to be resolvable even under ideal circumstances (Small & Isenberg, 1977). In protein studies, however, often only a single-exponential decay with a ϕ equal to the mean correlation time

$$\langle\phi\rangle = \left[\frac{\sum \beta_i/\phi_i}{\sum \beta_i}\right]^{-1} \tag{13}$$

is observed. The preexponential weighting factors, β_i, and therefore $\langle\phi\rangle$, are complicated functions of both the asymmetry of the protein and the orientation of the fluorophore's absorbance and emission dipoles with respect to the axes of the protein. For example, for a fluorophore that has coincident absorbance and emission dipoles and is attached to a prolate ellipsoid shaped protein, $\langle\phi\rangle$ will be maximal if the dipoles are aligned parallel to the long axis ($\theta_1 = 0$ in Figure 2) and minimal when the dipoles are aligned parallel to the short axis ($\theta_1 = 90°$ in Figure 2).

Because $\langle\phi\rangle$ depends on the orientation of the probe as well as the size, shape, and flexibility of the molecule, the rotation ratio, $\langle\phi\rangle/\phi_{sphere}$, places fewer constraints on the range of ellipsoids that can represent the behavior of the molecule than the friction ratio does. However, because the rotation ratio depends on asymmetry differently than the friction ratio does, the rotation ratio can be used to place further limits on the family of ellipsoids generated using the friction ratio. First, $\langle\phi\rangle$ is measured and the rotation ratio is calculated. Then, Perrin's equations are used to calculate the three rotational diffusion coefficients (D_a, D_b, D_c) and five correlation times for each of the members of the friction ratio-consistent table of ellipsoids. Finally, the range of ellipsoids consistent with both the friction and rotation ratios is determined. This is accomplished by evaluating, for each ellipsoid, whether a probe orientation can be found such that the β_i's (eq 13) weight the five exponentials so that the experimentally-determined rotation ratio is recovered. The equations for determining the β_i's for different probe angles are outlined by Belford et al. (1972).

In addition to limiting the range of ellipsoids which can represent the hydrodynamic behavior of a molecule, time-resolved fluorescence anisotropy decay data can provide important information regarding molecular flexibility or segmental motion which cannot be inferred from the sedimentation data. This is due to the short time frame (picoseconds to nanoseconds) over which rotation is measured. In time-resolved fluorescence anisotropy measurements, segmental motion of a region of the protein containing the probe will produce a component in the anisotropy decay with a correlation time less than ϕ_{sphere}. The appropriate equation for the anisotropy decay in this case is

$$r(t) = r_0[\gamma e^{-t/\phi_{segmental}} + (1-\gamma)]e^{-t/\phi_{global}} \tag{14}$$

where γ is a scaling factor between 0 and 1 [see Lakowicz (1983)]. In this equation, $\phi_{segmental}$ is the correlation time for depolarizing motions of a domain containing the probe and ϕ_{global} is the correlation time for the rotational motion of the protein as a whole. Anisotropy decay data are typically analyzed as a sum rather than a product of exponentials, so that the decay law in the presence of segmental flexibility is observed to be

$$r(t) = r_0[p_{short}e^{-t/\phi_{short}} + p_{long}e^{-t/\phi_{long}}] \tag{15}$$

where $p_{short} = \gamma$ and $p_{long} = 1 - \gamma$. Thus

$$\phi_{short}^{-1} = \phi_{segmental}^{-1} + \phi_{global}^{-1}; \quad \phi_{long}^{-1} = \phi_{global}^{-1} \tag{16}$$

An anisotropy decay which analyzes as a biexponential with one correlation time greater than or equal to ϕ_{sphere} and one less than ϕ_{sphere} can thus be diagnostic for segmental motion of a domain of the macromolecule containing the probe.

Proteins. Human recombinant VIIa was a generous gift of Dr. Ulla Hedner, Novo Nordisk, Copenhagen. Fluorescence anisotropy studies were performed using dansyl-labeled VIIa (DF-VIIa) covalently modified at its active site histidine with dansyl-D-Phe-L-Phe-Arg chloromethyl ketone as described previously (Waxman et al., 1992). Briefly, DF-VIIa was separated from free dansyl-FFRCk on a Sephadex G-15 column. Protein and dansyl concentrations were measured by absorbance, and the labeling ratio observed was 1 mol of dansyl to 1 mol of VIIa when VIIa was fully inhibited.[2] SDS–PAGE run under reducing conditions showed that the fluorescence label was bound exclusively to the heavy chain of VIIa as would be expected for this active site specific modification.

Studies of the TF·VIIa complex are complicated by the requirement that full-length TF be reconstituted in phospholipid vesicles or solubilized in detergent. This makes the possible interactions of TF and VIIa which involve the lipid or detergent difficult to resolve from those due strictly to direct protein–protein interactions and complicates the thermodynamic description of the TF·VIIa interaction. Furthermore, a hydrodynamic study of the complex would be difficult to interpret since global motions of the complex would be dominated by the overall motion of the lipid vesicles. In the present studies, we make use of a soluble TF (TF_{1-218}; sTF) which lacks the transmembrane and cytoplasmic domains. This material was prepared and purified as described previously (Waxman et al., 1992).

Ultracentrifugation Experiments. Sedimentation equilibrium studies of the sTF·VIIa complex were performed at 23.3 °C in a Beckman Model E analytical ultracentrifuge equipped with an electronic speed control, RTIC temperature controller,

[2] The extinction of human VIIa at 280 nm was based on the number of tryptophan and tyrosine residues in recombinant VIIa (Thim et al., 1988) using average extinction coefficients for tryptophan (5500 M^{-1} cm^{-1}) and tyrosine (1200 M^{-1} cm^{-1}) residues in a protein (Wetlaufer, 1962). The extinction of DF-VIIa was calculated using the extinction coefficients for ϵ-dansyllysine in water (J. B. A. Ross, unpublished data) and our calculated value for the extinction of VIIa at 280 nm, assuming additivity of the absorptions.

Rayleigh interference optics, and a pulsed laser diode light source (670 nm). Data were acquired using a television-camera-based, on-line data acquisition and analysis system (Laue, 1981; Laue et al., 1992). Samples were loaded into short column cells (0.7 mm) (Yphantis, 1960) at several concentrations up to 1 mg/mL total protein. Data were collected at intervals after the estimated equilibrium time and tested for equilibrium by subtracting successive scans (Yphantis, 1964). M_r was estimated using the nonlinear least-squares analysis program NONLIN (Johnson et al., 1981) as described previously (Laue et al., 1984).

Sedimentation velocity experiments were performed on a Beckman XLA analytical centrifuge equipped with absorption optics that allow scanning at multiple wavelengths and interfaced to a microcomputer for data acquisition. The sedimentation coefficient was determined from the movement of the boundry (Stafford, 1992) and corrected to standard conditions (20.0 °C) and zero protein concentration using conventional methods (van Holde, 1985; Teller, 1973).

Fluorescence Experiments. Time-resolved fluorescence intensity and anisotropy measurements were obtained by the time-correlated single-photon counting method using an instrument previously described (Hasselbacher et al., 1991a). Decay curves were collected into either 2000 or 4000 channels, yielding a resolution of 22 or 11 ps/channel, respectively. Fluorescence decays were measured using excitation at 330 nm with detection through a 10-nm band-pass filter centered at 530 nm and a polarizer set vertically, horizontally, or at the magic angle (Badea & Brand, 1979). Fluorescence decay data were analyzed using nonlinear least-squares regression (Bevington, 1969). The fluorescence intensity decay collected at the magic angle, $I_m(t)$, was fit to a sum of exponentials given by

$$I_m(t) = \sum_{i=1}^{n} \alpha_i e^{-t/\tau_i} \quad (17)$$

where τ_i is the lifetime and α_i is the amplitude of the ith component. The intensity-weighted mean lifetime, $\langle\tau\rangle$, is defined by the relationship

$$\langle\tau\rangle = \sum_{i=1}^{n} \alpha_i \tau_i^2 / \sum_{i=1}^{n} \alpha_i \tau_i \quad (18)$$

The decay of the emission anisotropy was analyzed as a sum of exponentials (eq 12). The anisotropy parameters were obtained by fitting the vertically and horizontally polarized emission decay curves ($I_v(t)$ and $I_h(t)$), using an approach similar to that described by Cross and Fleming (1984). To help constrain the intensity decay parameters (eq 17) and provide a means for scaling the $I_v(t)$ and $I_h(t)$ curves to each other, we included the $I_m(t)$ curve in the analysis and fit all the data simultaneously according to the following relationships:

$$I_v(t) = {}^1/_3 I_m(t)\,(1 + 2\sum \beta_j e^{-t/\phi_j}) \quad (19)$$

$$I_h(t) = {}^1/_3 I_m(t)\,(1 - \sum \beta_j e^{-t/\phi_j})$$

RESULTS

Intensity Decay Measurements. Intensity decay measurements were performed using 6 μM DF-VIIa alone and in the presence of 10 μM sTF. Measurements were performed in 0.05 M Tris buffer, 0.1 M NaCl, and 5 mM $CaCl_2$, pH 7.5. No free DF-VIIa is expected in the sample containing sTF as the dissociation constant (0.59 nM) is well below the concentrations used (Waxman et al., 1992). The intensity-weighted mean fluorescence lifetimes, $\langle\tau\rangle$, ranged from 11.1 ns at 25 °C to 12.4 ns at 5 °C. No change in $\langle\tau\rangle$ was seen upon addition of sTF. The relatively long $\langle\tau\rangle$ compared to literature values for dansylated proteins [see Hasselbacher et al. (1991b)] and the small dependence of $\langle\tau\rangle$ on temperature both suggest that the dansyl group is shielded from solvent as would be expected if it were buried in the active site of VIIa. In addition, the emission spectrum of DF-VIIa is blue-shifted approximately 12 nm relative to that of ε-dansyllysine. This is consistent with the suggestion that the dansyl group is buried in the active site.

Table I: Calculation of Hydrodynamic Parameters[a]

parameter	VIIa	sTF·VIIa
M_r[b]	49000	73700
R_p (cm)	2.50×10^{-7}	2.80×10^{-7}
V_p (mL)	6.20×10^{-20}	9.40×10^{-20}
$\bar{v}$ (mL/g)	0.703	0.711
δ	0.28	0.28
V (mL)	8.70×10^{-20}	1.30×10^{-19}
R_{sphere} (cm)	2.80×10^{-7}	3.20×10^{-7}
f_{sphere} (g/s)	5.20×10^{-8}	5.90×10^{-8}
$s^{\circ}_{20,w}$[c] (s)	3.40×10^{-13}	3.90×10^{-13}
f (g/s)	7.20×10^{-8}	9.10×10^{-8}
f/f_{sphere}[d]	1.39	1.52
ϕ_{sphere}[e] (ns)	22	32
$\langle\phi\rangle$[e] (ns)	94	123
$\langle\phi\rangle/\phi_{sphere}$	4.27	3.73

[a] Values have been rounded off for the purpose of presentation. [b] The estimated error in M_r is ±2%. [c] The estimated error in s is $\pm 0.1 \times 10^{-13}$ s. [d] Propagation of error indicates a ±3% error in f/f_{sphere}. Intermediate values were not rounded for the actual calculations. [e] Correlation times presented are for 20 °C.

Recognizing that the dansyl probe is specifically placed, we make the assumption that each of the lifetime components of the intensity decay is associated with the same molecular motions of the protein. In this case, the mean lifetime, $\langle\tau\rangle$, conveys no less information than the individual decay components. Consequently, the $\langle\tau\rangle$ of 11.1 ns at 25 °C may be used to generate apparent rotational correlation times from steady-state anisotropy values for DF-VIIa and sTF·DF-VIIa obtained previously (Waxman et al., 1992). In that study, the steady-state anisotropy at 25 °C was 0.234 for DF-VIIa alone and 0.254 for DF-VIIa in the presence of saturating amounts of sTF. This anisotropy change could be reversed by addition of EDTA. Using eq 9 and an $\langle r\rangle_0$ of 0.32 for the dansyl probe (obtained from a Perrin plot of DF-VIIa) yields apparent mean rotational correlation times of 30 and 43 ns for DF-VIIa and sTF·DF-VIIa, respectively. From eq 7, the rotational correlation times of hydrated spheres (0.28 g of water/g of protein) with the same molecular weights as these species would be 22 and 32 ns, respectively. These data suggest that the shapes of DF-VIIa and the sTF·DF-VIIa complex are not well represented by hydrated spheres. Considering the assumptions involved, it is impossible to determine from these data whether the large correlation times are due to asymmetry or higher order association. To resolve this question, we turned to ultracentrifugation experiments.

Ultracentrifugation Studies. Table I shows the results obtained at each step of the procedure described in the Experimental Procedures section and outlined in Figure 1. The M_r values obtained from equilibrium ultracentrifugation of VIIa, sTF, and an equimolar mixture of sTF and VIIa were 49 000, 27 700, and 73 700, respectively. These values are consistent with those obtained previously (Waxman et al., 1992). As before, neither sTF nor VIIa shows a tendency toward reversible self-association at the concentrations employed. No dissociation of the sTF·VIIa complex was observed

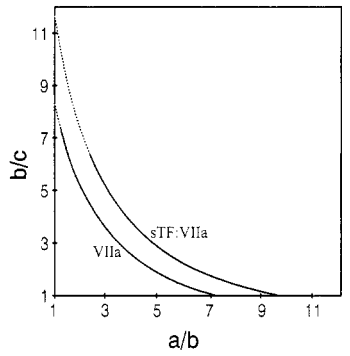

FIGURE 3: Flatness (b/c) versus elongation (a/b) for the family of ellipsoids consistent with the friction ratios determined for VIIa and sTF·VIIa. The solid part of the curves represents the subset of ellipsoids consistent with both the friction and rotation ratios.

at these concentrations, consistent with the dissociation constant of 0.59 nM previously obtained (Waxman et al., 1992).

Sedimentation velocity experiments performed using VIIa and the equimolar mixture of sTF and VIIa both showed a single boundary. The translational frictional coefficients shown in Table I are calculated according to eq 6. f_{sphere} for VIIa and sTF·VIIa are shown for comparison and the friction ratios f/f_{sphere} are calculated. As discussed above, each friction ratio is consistent with a family of ellipsoidal shapes ranging from prolate to oblate. For VIIa alone, the axial ratios for the oblate and prolate ellipsoids consistent with the determined friction ratio are 8.4 and 7.2, respectively. For sTF·VIIa, the axial ratios are 11.8 and 9.6 for the oblate and prolate ellipsoids.[3] Figure 3 shows b/c versus a/b for the family of ellipsoids consistent with the friction ratios obtained. In examining this figure, it is useful to note that the intercepts of the friction ratio-consistent curve at $a/b = 1$ and $b/c = 1$ represent the oblate and prolate ellipsoids, respectively. Clearly, VIIa and sTF·VIIa are both highly asymmetric. Furthermore, the friction ratio for sTF·VIIa exceeds that of VIIa alone. However, as discussed above, the translational frictional coefficients alone are not sufficient to distinguish among the family of ellipsoids, nor are they capable of distinguishing between a highly asymmetric flexible molecule and a rigid molecule with lower asymmetry. We therefore performed fluorescence anisotropy decay measurements to narrow further the range of ellipsoids which are consistent with the hydrodynamic behavior of VIIa and sTF·VIIa and to assess the extent to which segmental motions may be occurring.

Fluorescence Anisotropy Decay Studies. The results from the time-resolved fluorescence anisotropy experiments with DF-VIIa and sTF·DF-VIIa are shown in Table II. Conditions were identical to those used for the intensity decay measurements. In all data sets where DF-VIIa was observed alone, a biexponential model was necessary to fit the data. Although the preexponential of the shorter lived decay component was consistently only about 10% that of the longer lived decay component, the quality of the fit was clearly improved by the addition of this component. As noted above, the ϕ_{sphere} for VIIa at 20 °C is 22 ns. When this value is compared to the

[3] One reviewer questioned how the choice of eq 1 rather than eq 2 for the calculation of the radius of an unhydrated spherical protein could alter our results. The use of eq 2 would yield unhydrated radii that are 2–4% smaller than those calculated using eq 1. Use of these smaller radii in subsequent calculations would yield axial ratios approximately 5–10% larger and would suggest that VIIa and the sTF·VIIa complex are even more asymmetric. The general conclusions of the paper, however, are unaffected by personal preference regarding eqs 1 or 2.

Table II: Time-Resolved Fluorescence Anisotropy Parameters[a]

sample	T (°C)	η (cP)	β_1	ϕ_1 (ns)	β_2	ϕ_2 (ns)
DF-VIIa	5	1.56	0.36	145	0.04	22.0
	10	1.35	0.36	126	0.04	18.6
	15	1.17	0.36	108	0.04	16.1
	20	1.04	0.36	97	0.04	14.1
	25	0.91	0.36	85	0.04	9.6
sTF·DF-VIIa	5	1.56	0.40	194		
	10	1.35	0.39	168		
	15	1.17	0.40	141		
	20	1.04	0.40	122		
	25	0.91	0.40	112		

[a] The results presented for DF-VIIa were obtained by fixing each β_i to the average value obtained from unrestricted analyses as described in the Results Section. The results presented for sTF·DF-VIIa are values obtained from completely unrestricted analyses.

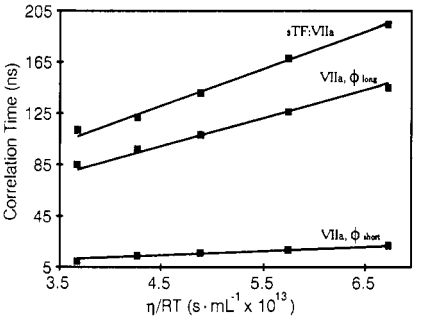

FIGURE 4: Correlation times versus η/RT for DF-VIIa and sTF·DF-VIIa. A single-exponential model fit the anisotropy decay of sTF·DF-VIIa. Both the long and short correlation times for the biexponential model used for DF-VIIa alone are shown. Details are described in Results.

correlation times obtained at this temperature, it can be seen that the 97-ns correlation time is considerably larger than ϕ_{sphere}, and the 14-ns correlation time is considerably smaller than ϕ_{sphere}. This pattern suggests that the anisotropy decay of DF-VIIa is composed of decays due to global and segmental motions. From eqs 14–16, it can be seen that the larger correlation time is equal to global motion correlation time, ϕ_{global}. A simple calculation (eq 16) shows that the segmental motion correlation time is 12 ns. Equation 7 can be used to make an order of magnitude approximation of the size of the protein domain responsible for the fast component of the anisotropy decay. This analysis yields a molecular weight of approximately 30 000 and suggests that a significant fraction of the protein is involved. In addition, it is consistent with the other spectroscopic evidence that indicates that the dansyl probe is buried in the active site of VIIa.

Figure 4 shows the temperature and viscosity dependence of ϕ_{long} and ϕ_{short}. The correlation times used for this graph were obtained by fixing β_{long} and β_{short} to the average of their respective values obtained from initial analyses where all fitting parameters were iterated. The fitting statistics were unchanged by this procedure, and the reproducibility of the correlation times was greatly improved. Also, the behavior of the correlation times as a function of η/T obeys the Stokes–Einstein equation (eq 7) as would be expected if the correlation times reflected a global rotation and a large-scale segmental motion of DF-VIIa. The observed dependence of the shorter correlation time on solution viscosity is particularly notable as it would not be expected if the faster component of the anisotropy decay were due to rapid motion of the probe within the active site of VIIa. The large value for ϕ_{long} as compared to ϕ_{sphere} is further evidence that DF-VIIa is highly asymmetric.

In contrast to the data obtained for DF-VIIa alone, the anisotropy decay of the sTF·DF-VIIa complex was best

modeled as a single exponential. There was no improvement in any of the fitting statistics criteria when a biexponential model was used for analysis. In fact, when the data for the complex were analyzed by a biexponential model, degenerate correlation times were obtained. At 20 °C, ϕ_{sphere} for sTF·DF-VIIa is 32 ns. By contrast, the correlation time obtained from analysis of the anisotropy decay is 122 ns, indicating, in agreement with the sedimentation data, that sTF·DF-VIIa is also highly asymmetric. Figure 4 also shows the temperature and viscosity dependence of the correlation time of the sTF·DF-VIIa complex. As observed for DF-VIIa alone, the dependence of the correlation time on η/T obeys the Stokes–Einstein equation (eq 7).

In the final step of the analysis outlined in the Experimental Procedures section, we used Perrin's equations as outlined by Small and Isenberg (1977) to generate the three principal rotational diffusion constants and five rotational correlation times for the family of ellipsoids consistent with the friction ratios obtained for VIIa and sTF·VIIa (Table I). We then determined the subset of each family that was consistent with both the rotation and friction ratios (Figure 3). For VIIa alone, the ellipsoids consistent with both the friction and rotation ratios range from the prolate to an ellipsoid with axial ratios of a/b and b/c of 1.3 and 7.2, respectively. The corresponding molecular axes are 204 × 28 × 28 Å for the prolate ellipsoid and 126 × 98 × 14 Å for the other limiting shape. For sTF·VIIa, the ellipsoids consistent with both the friction and rotation ratios range from the prolate to an ellipsoid with axial ratios of a/b and b/c of 2.37 and 6.41, respectively. The corresponding molecular axes are 254 × 26 × 26 Å for the prolate ellipsoid and 186 × 78 × 12 Å for the other limiting shape. Thus, for both VIIa and sTF·VIIa, a subset of flattened shapes is eliminated when the rotation ratio is taken into account. In particular, this analysis clearly demonstrates that an oblate model cannot account for the hydrodynamic behavior of either VIIa or its complex with sTF.

DISCUSSION

In vivo, complexation of TF and VIIa takes place at the vascular wall (Nemerson & Turitto, 1991). Shear stresses from blood flow in this region are high. Evidence from enzyme kinetic studies of TF·VIIa in a flowing reactor system suggests that the intrinsic activity of the complex is strongly affected by these shearing effects (Gemmell et al., 1990). Possible mechanisms for this effect include shear-induced conformational change or an increase in the probability of successful collisions due to preferred orientations of the enzyme and substrate under conditions of flow. Either mechanism, of course, would require that some or all of the molecules are asymmetric. With regard to this, several studies have provided evidence that suggest that other members of the clotting factor family are asymmetric (Lim et al., 1977; Laue et al., 1984; Isaacs et al., 1986; Husten et al., 1987; Luckow et al., 1989; Olsen et al., 1992). In this paper, we have investigated the hydrodynamic properties of VIIa and sTF·VIIa by sedimentation velocity and fluorescence anisotropy decay measurements. The combined data clearly demonstrate that VIIa and the complex it forms with sTF are highly asymmetric.

In addition, the anisotropy decay data show differences in the conformational dynamics of VIIa alone and bound to sTF. Specifically, a biexponential model is necessary to adequately describe the decay of the fluorescence anisotropy of VIIa. Multiexponential anisotropy decays have been observed for proteins which exhibit segmental flexibility. For example, Yguerabide et al. (1970) observed a biexponential decay with correlation times of 33 and 168 ns for dansyllysine bound to IgG. The longer correlation time, which exceeds ϕ_{sphere} for the 150 000-Da protein, was attributed to the global rotation of the protein while the shorter correlation time, which is less than ϕ_{sphere}, was attributed to segmental motions of the Fab fragments. That result is essentially identical with what we have observed for VIIa in the absence of sTF. The shorter correlation time, 14 ns at 20 °C, is significantly less than ϕ_{sphere} but substantially longer than expected for side chain motions (<1 ns). It is likely that this short correlation time represents the jointed motion of a structural domain of VIIa that contains the labeled active site.

It could be argued that the improvement in the statistics obtained when the anisotropy decay of DF-VIIa is fit to a biexponential decay law reflects the presence of three potentially resolvable anisotropy decay constants and not the presence of segmental motion. To test this possibility, we analyzed simulated data created with an intensity decay identical to that observed for DF-VIIa and anisotropy decay parameters corresponding to those of several of the rigid ellipsoids consistent with the mean correlation time of VIIa. All correlation times recovered were greater than or equal to ϕ_{sphere}. Thus, the anisotropy decay data indicate that a structural domain of VIIa that contains the active site undergoes segmental motions. Moreover, the anisotropy decay data indicate that these motions are damped when VIIa binds sTF. We suggest that this stabilization by the cofactor, TF, of a limited number of conformations of the enzyme VIIa is important for proper recognition of the substrate factor X.

ACKNOWLEDGMENT

We appreciate the technical assistance of Theresa M. Ridgeway, Daryl Lyons, and Steven Eaton, and we acknowledge the scientific contributions of Dr. Arabinda Guha, Dr. Carol Hasselbacher, and Dr. Donald Senear. We also thank one of the reviewers for his careful attention and helpful suggestions.

REFERENCES

Bach, R. (1988) *CRC Crit. Rev. Biochem. 23*, 339–368.

Badea, M. G., & Brand, L. (1979) *Methods Enzymol. 61*, 378–425.

Belford, G. G., Belford, R. L., & Weber, G. (1972) *Proc. Natl. Acad. Sci. U.S.A. 69*, 1392–1393.

Bevington, P. R. (1969) *Data Reduction and Error Analysis for the Physical Sciences*, pp 204–246, McGraw-Hill, New York, NY.

Cohn, E. J., & Edsall, J. T. (1943) *Proteins, Amino Acids and Peptides as Ions and Dipolar Ions*, p 157, Rheinhold, New York, NY.

Cross, A. J., & Fleming, G. R. (1984) *Biophys. J. 46*, 45–56.

Gemmell, C. H., Broze, G. J., Jr., Turitto, V. T., & Nemerson, Y. (1990) *Blood 76*, 2266–2271.

Hasselbacher, C. A., Waxman, E., Galati, L., Contino, P., Ross, J. B. A., & Laws, W. R. (1991a) *J. Phys. Chem. 95*, 2995–3005.

Hasselbacher, C. A., Schwartz, G. P., Glass, J. D., & Laws, W. R. (1991b) *Int. J. Pept. Protein Res. 38*, 459–468.

Husten, J. E., Esmon, C. T., & Johnson, A. E. (1987) *J. Biol. Chem. 27*, 12953–12961.

Isaacs, B. S., Husten, E. J., Esmon, C. T., & Johnson, A. E. (1986) *Biochemistry 25*, 4958–4969.

Johnson, M. L., Correia, J. C., Yphantis, D. A., & Halvorson, H. R. (1981) *Biophys. J. 36*, 575–588.

Lakowicz, J. R. (1983) *Principles of Fluorescence Spectroscopy*, pp 161–162, Plenum Press, New York, NY.

Laue, T. M. (1981) Ph.D. Dissertation, University of Connecticut, Storrs, CT.

Laue, T. M., Johnson, A. E., Esmon, C. T., & Yphantis, D. A. (1984) *Biochemistry 23*, 1339–1348.
Laue, T. M., Shah, B. D., Ridgeway, T. M., & Pelletier, S. M. (1992) *Analytical Ultracentrifugation in Biochemistry and Polymer Science* (Harding, S., & Rowe, A., Eds.) pp 90–125, Royal Society of Chemistry, London.
Lim, T. K., Bloomfield, V. A., & Nelsestuen, G. L. (1977) *Biochemistry 25*, 4177–4181.
Luckow, E. A., Lyons, D. A., Ridgeway, T. M., Esmon, C. T., & Laue, T. M. (1989) *Biochemistry 28*, 2348–2354.
Nemerson, Y., & Turitto, V. T. (1991) *Thromb. Haemostasis 66*, 272–276.
Olsen, P. H., Esmon, N. L., Esmon, T., & Laue, T. M. (1992) *Biochemistry 31*, 746–754.
Perrin, F. (1934) *J. Phys. Radium, Ser. VII, V*, 497–511.
Pessen, H., & Kumosinski, T. F. (1985) *Methods Enzymol. 117*, 219–255.
Silverberg, S. A., Nemerson, Y., & Zur, M. (1977) *J. Biol. Chem. 252*, 8481–8488.
Small, E. W., & Isenberg, I. (1977) *Biopolymers 16*, 1907–1928.
Stafford, W. F., III (1992) *Anal. Biochem. 203*, 295–301.
Stafford, W. F., III, & Szent-Györgyi, A. G. (1978) *Biochemistry 17*, 607–614.
Tao, T. (1969) *Biopolymers 8*, 609–632.
Teller, D. C. (1973) *Methods Enzymol. 27*, 346–441.
Teller, D. C. (1976) *Nature 260*, 729–731.
Thim, L., Bjoern, S., Christensen, M., Nicolaisen, E. M., Lund-Hansen, T., Pedersen, A. H., & Hedner, U. (1988) *Biochemistry 27*, 7785–7793.
van Holde, K. E. (1985) *Physical Biochemistry*, 2nd ed. p 117, Prentice-Hall, Englewood Cliffs, NJ.
Waxman, E., Ross, J. B. A., Laue, T. M., Guha, A., Thiruvikraman, S. V., Lin, T. C., Konigsberg, W. H., & Nemerson, Y. (1992) *Biochemistry 31*, 3998–4003.
Wetlaufer, D. B. (1962) *Adv. Protein Chem. 17*, 303–390.
Yguerabide, J., Epstein, H. F., & Stryer, L. (1970) *J. Mol. Biol. 51*, 573–590.
Yphantis, D. A. (1960) *Ann. N.Y. Acad. Sci. 88*, 586–601.
Yphantis, D. A. (1964) *Biochemistry 3*, 297–317.